

# Analysis of a hollow core photonic bandgap fiber ring resonator based on micro-optical structure

Lishuang Feng,<sup>1,2</sup> Xiaoyuan Ren,<sup>1,2,\*</sup> Xuewen Deng,<sup>2</sup> and Huilan Liu<sup>1</sup>

<sup>1</sup>Laboratory on Inertial Science and Technology, Beihang University, Beijing 100191, China

<sup>2</sup>Laboratory of Micro-nano Measurement-Manipulation and Physics, Beihang University, Beijing 100191, China  
\*renxiaoyuan1984@163.com

**Abstract:** The fiber ring resonator (FRR) is the key component of resonator fiber optic gyros (R-FOGs). The configuration of a novel hollow core photonic bandgap fiber (HC-PBF) ring resonator is proposed based on the usage of micro-optical structure. The normalized transfer function of such kind of FRR is derived, and the effects of different FRR parameters' on the resonant depth, resonant finesse and sensitivity limited by the shot noise of the detector are simulated. The laboratory sample of integrated HC-PBF ring resonator is fabricated and tested experimentally and the optimal scheme is proposed based on the acquired test data. The experimental setup and results verify the feasibility of the micro-optical coupling structure used in the HC-PBF ring resonator and also support the integration and miniaturization of R-FOGs composed of HC-PBFs.

©2012 Optical Society of America

**OCIS codes:** (060.2340) Fiber optics components; (060.2370) Fiber optics sensors; (060.2800) Gyroscopes; (060.4005) Microstructured fibers.

---

## References and links

1. H. C. Lefèvre, *The Fiber-Optic Gyroscope* (National Defense Industry & Beijing, 2002), Chap. 2.
2. N. Barbour, "Inertial components-past, present and future," presented at 2001 American Institute of Aeronautics & Astronautics Guidance, Navigation and Control Conference, Montreal, Canada, 6–9 Aug. 2001.
3. S. P. Divakaruni and S. J. Sanders, "Fiber-optic gyros -a compelling choice for high precision applications," presented at the 18th International Conference on Optical Fiber Sensors, Cancún, Mexico, 23 Oct. 2006.
4. K. Iwatsuki, K. Hotate, and M. Higashiguchi, "Kerr effect in an optical passive ring-resonator gyro," *J. Lightwave Technol.* **4**(6), 645–651 (1986).
5. K. Hotate, "Future evolution of fiber optic gyros," *Opt. Rev.* **4**(1), A28–A34 (1997).
6. K. Iwatsuki, K. Hotate, and M. Higashiguchi, "Effect of Rayleigh backscattering in an optical passive ring-resonator gyro," *Appl. Opt.* **23**(21), 3916–3924 (1984).
7. C. M. Smith, N. Venkataraman, M. T. Gallagher, D. Müller, J. A. West, N. F. Borrelli, D. C. Allan, and K. W. Koch, "Low-loss hollow-core silica/air photonic bandgap fibre," *Nature* **424**(6949), 657–659 (2003).
8. G. A. Sanders, L. K. Strandjord, and T. Qiu, "Hollow core fiber optic ring resonator for rotation sensing," presented at the 18th International Conference on Optical Fiber Sensors, Cancún, Mexico, 23 Oct. 2006.
9. M. A. Terrel, M. J. F. Dignonnet, and S. Fan, "Resonator fiber optic gyroscope using an air-core fiber," *J. Lightwave Technol.* **30**(7), 931–937 (2012).
10. H. K. Kim, M. J. F. Dignonnet, and G. S. Kino, "Air-Core Photonic-Bandgap Fiber-Optic Gyroscope," *J. Lightwave Technol.* **24**(8), 3169–3174 (2006).
11. T. P. Hansen, J. Broeng, C. Jakobsen, G. Vienne, H. R. Simonsen, M. D. Nielsen, P. M. W. Skovgaard, J. R. Folkenberg, and A. Bjarklev, "Air-guiding photonic bandgap fibers: spectral properties, macrobending loss, and practical handling," *J. Lightwave Technol.* **22**(1), 11–15 (2004).
12. X. L. Zhang, W. Jin, and D. Q. Ying, "Performance analysis of an optical passive ring-resonator gyro with a hollow-core photonic bandgap fiber sensing coil," *Proc. SPIE* **7853**, 785324, 785324-9 (2010).
13. V. Dangui, M. J. F. Dignonnet, and G. S. Kino, "Laser-driven photonic-bandgap fiber optic gyroscope with negligible Kerr-induced drift," *Opt. Lett.* **34**(7), 875–877 (2009).
14. T. Dang, G. A. Sanders, and T. Spicer, "Micro-optics photonic bandgap fiber coupler," United states Patent, US 7680372 B2 (2010).
15. R. E. Meyer, S. Ezekiel, D. W. Stowe, and V. J. Tekippe, "Passive fiber-optic ring resonator for rotation sensing," *Opt. Lett.* **8**(12), 644–646 (1983).

---

## 1. Introduction

The Fiber optic gyroscope (FOG) is one of the most typical angular velocity sensor based on Sagnac effect [1]. Currently, interferometric fiber optic gyroscope (I-FOG) technology is

relatively mature, and it is widely used in inertia navigation, oil drilling and robot control [2]. However, the large length of I-FOG resonator is disadvantageous to the compactness of gyro. I-FOGs are very sensitive to their surrounding environment, therefore, they require an optimized structure and thermal design, winding of the sensing coil in a special pattern, a better scheme of signal detection and effective shielded technology. All of these requirements result in I-FOGs with complicated structures and high costs [3]. Compared with I-FOGs, R-FOGs use a FRR to measure the angular velocity, which takes advantages such as a shorter fiber length and good linearity with wide dynamic range [4]. However, the R-FOG using a normal fiber is sensitive to external stress and temperature, and requires the use of a highly coherent source [5], resulting in large and easily-aroused noise [4, 6]. To counteract these effects, the use of a sensing coil composed of HC-PBF has been proposed in the design of R-FOGs [7–9]. The Kerr effect, Faraday effect and Rayleigh scattering effect of the HC-PBF are expected to be suppressed by two to three orders of magnitude compared with a normal fiber [10]. In addition, HC-PBF is insensitive to macrobending over the majority of the bandgap, therefore, the radius of the sensing coil composed of HC-PBF can be decreased to several millimeters [11]. In summary, the integration and miniaturization of a high-accuracy RFOG based on HC-PBF is possible in the future [12].

The coupling between a HC-PBF and a normal fiber is still a tough issue. Although the traditional coupling approaches include fused coupling and lapped coupling between different fibers [8, 13]. The coupling loss of these two coupling approaches is relatively larger, and the optical alignment process is not easy to perform in practical operation. Fortunately, a type of micro-optics photonic bandgap fiber coupler based on existing micro-optics devices was proposed recently [14], and it was useful for the coupling of HC-PBFs and normal fibers. Owing to the rapid progress of the micro-fabrication technology, we propose a new type of coupling structure based on a micro-optical splitter and apply it to the ring resonator. Firstly, the theoretical derivation and simulation of the FRR model was performed. The sample of the coupler and FRR was subsequently fabricated and tested experimentally. Finally, the experimental results were analyzed and the optimized sample structure was presented.

## 2. Design of FRR based on micro-optical structure

### 2.1 Mathematical model of the FRR

Figure 1 provides a schematic of the HC-PBF ring resonator based on micro-optical structure. Ports 1 and 4 connected with the PMFs are the input and output ports respectively. Ports 2 and 3 are the HC-PBF connected with the FRR. The PMF and HC-PBF are held in place by the double-core capillaries *g* and *h*. The input and output light waves converge and are collected by the collimating lens *c*, *e*, and *d*, *f*, respectively. The micro-optical splitter serves as the fiber coupler here. The light through the splitter is split by plating the highly reflective membrane *b* near the side of the HC-PBF and the highly anti-reflective membrane *a* near the side of the PMF. All of the fibers are assumed to be polarization maintaining, therefore, the influence of polarization is not considered here.

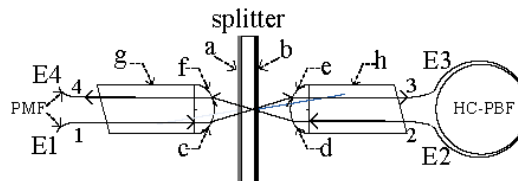


Fig. 1. Schematic of the HC-PBF ring resonator based on micro-optical structure.

The transmissivity of the highly anti-reflective membrane *a* is  $T_a$ , and the reflectivity of the highly reflective membrane *b* is  $R_b$ , where  $k = 1 - R_b$ . When light propagates from one collimating lens to another, an identical coupling loss  $\alpha_c$  between port 1 and port 3, port 1 and port 4, or port 2 and port 3 is assumed. The HC-PBF is *L* in length, and with loss coefficient

$\alpha_f$ , and refraction index  $n$ . The central angular frequency and the linewidth of the laser source are  $\omega$  and  $\Delta\omega$ , respectively. When light enters the splitter, a portion of the light is reflected and the rest is transmitted directly. The multi-beam interference is formed at the output port. According to the multi-beam interference theory, the expression for the electric field of output lightwave is

$$E_4 = E_0 T_a e^{i\omega t} [T e^{i\phi(t)} + R' \sum_{m=1}^{\infty} (-1)^{m-1} (Q')^{m-1} e^{-i\omega m t} e^{i\phi(t-m\tau)}] \quad (1)$$

where  $T = \sqrt{(1-\alpha_c)(1-k)}$ ,  $R' = (1-\alpha_c)k e^{-\alpha_f L/2}$ ,  $Q' = \sqrt{(1-\alpha_c)(1-k)} e^{-\alpha_f L/2}$ , and  $m$  is an integer.

As Eq. (1) is given in accordance with the transfer function of normal fiber coupler FRR, the expressions for the following several definitions can be derived accordingly.

- The normalization transfer function  $T_{\text{FRR}}$  is

$$T_{\text{FRR}} = \left| \frac{E_4}{E_1} \right|^2 = T_a^2 \left( T^2 + \frac{2TR(\cos \omega\tau + Q)}{1+Q^2 + 2Q \cos \omega\tau} + \frac{(R')^2}{1-(Q')^2} \cdot \frac{1-Q^2}{1+Q^2 + 2Q \cos \omega\tau} \right) \quad (2)$$

where  $\tau = Ln/c$ ,  $Q = \sqrt{(1-\alpha_c)(1-k)} e^{-\Delta\omega\tau - \alpha_f L/2}$ , and  $R = k(1-\alpha_c) e^{-\Delta\omega\tau - \alpha_f L/2}$ . With Eq. (2), one can obtain the maximum and minimum values of  $T_{\text{FRR}}$ ,

$$T_{\text{FRR}}^{\max} = T_a^2 \left( T^2 + \frac{2TR}{1+Q} + \frac{(R')^2}{1-(Q')^2} \cdot \frac{1-Q}{1+Q} \right) \quad T_{\text{FRR}}^{\min} = T_a^2 \left( T^2 - \frac{2TR}{1-Q} + \frac{(R')^2}{1-(Q')^2} \cdot \frac{1+Q}{1-Q} \right) \quad (3)$$

- The resonant depth  $\rho$  is

$$\rho = \frac{T_{\text{FRR}}^{\max} - T_{\text{FRR}}^{\min}}{T_{\text{FRR}}^{\max}} \quad (4)$$

- Here it is assumed that  $A = R'^2/(1-Q'^2)$ ,  $B = 1-Q^2$ , and  $C = 1+Q^2$ , therefore the resonant finesse  $F$  is

$$F = \frac{\pi}{\cos^{-1} \left( \frac{AB^2 + 2TRQB - AC^2 + 2TRQC}{ATRQ^2 - 2QAC + 2TRB} \right)} \quad (5)$$

- In the R-FOG, the sensitivity limited by the shot noise of detector is given by [15]

$$\Delta\Omega \approx \frac{\lambda P \sqrt{2}\Gamma}{4A' \text{SNR}} \quad (6)$$

where  $P$  is the perimeter of single-fiber loop,  $A'$  is the area enclosed by the FRR,  $\Gamma$  is the resonant linewidth, and  $\text{SNR}$  is the signal-to-noise ratio of the system.

## 2.2 Simulation

In this section, the effects of the micro-optical splitter structure on the resonant depth  $\rho$ , resonant finesse  $F$  and sensitivity  $\Delta\Omega$  are simulated. The structural effects evaluated include the reflectivity of the highly reflective membrane  $R_b$ , the coupling loss  $\alpha_c$ , and the laser linewidth  $\Delta\omega$ . It is assumed that  $R_b = 0.9$ ,  $\alpha_c = 0.1$ ,  $\Delta\omega = 30$  kHz,  $L = 1.6$  m,  $T_a = 0.99$ ,  $\alpha_f = 0.0039$  m<sup>-1</sup>,  $\lambda = 1.55$   $\mu\text{m}$ ,  $n = 0.99$ , the quantum efficiency of photo-detector  $\eta = 99\%$ , the integral time  $t = 10$  s, and  $A = 0.20$  m<sup>2</sup>.

The effects of  $R_b$ ,  $\alpha_c$ , and  $\Delta\omega$  on the resonant depth  $\rho$  are illustrated in Fig. 2. In Fig. 2(a),  $\rho$  increases and then decreases as  $\alpha_c$  increases, and it reaches a maximum of 0.9977 when the optimal resonant condition,  $R_b + \alpha_c = 1$ , is satisfied. In general, when the optimal resonant condition is satisfied, the loss refers to the total loss of the resonator, however, the loss considered here represents mainly the coupling loss. When  $R_b$  becomes smaller, the curve of the resonant depth becomes more smooth, and  $\rho$  decreases as  $R_b$  increases when  $\alpha_c > 0.15$ . When  $R_b$  and  $\alpha_c$  satisfy the optimal resonant condition,  $\rho$  decreases nearly linearly as  $\Delta\omega$  increases (Fig. 2(b)). When  $\Delta\omega$  is smaller than 1 MHz,  $\rho$  can increase to more than 0.95, in contrast,  $\rho$  is reduced to 0.67 when  $\Delta\omega$  is 10 MHz. In fact, the resonant property of the FRR is affected by the factor  $\exp(-\Delta\omega/\omega')$ , which depends on the laser linewidth  $\Delta\omega$  and the resonance frequency  $\omega'$  of the resonator. For example, for  $L = 1.6$  m,  $\omega' = 189$  MHz,  $\Delta\omega = 1$  MHz, and  $\exp(-\Delta\omega/\omega') = 0.9947$ , the resonant property is only slightly affected by the laser linewidth. This effect will increase exponentially as  $\Delta\omega$  increases. The key factor that determines whether a larger  $\rho$  can be obtained is whether  $R_b$  and  $\alpha_c$  satisfy the optimal resonant condition. When  $\Delta\omega$  is less than 1 MHz, its influence can be neglected.

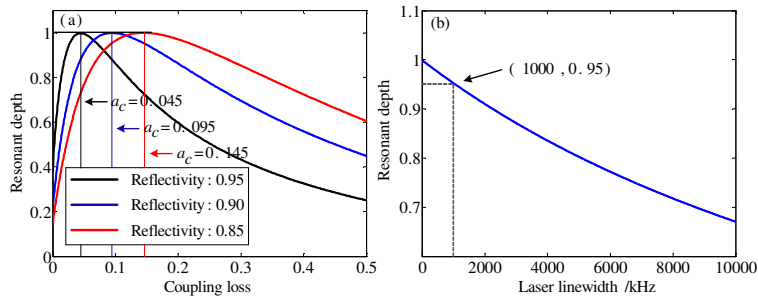


Fig. 2. Resonant depth varies with different optical parameters: (a) reflectivity and coupling loss and (b) laser linewidth.

Figure 3 plots the relations between the resonant finesse and different optical parameters, including  $R_b$ ,  $\alpha_c$ , and  $\Delta\omega$ . In Fig. 3(a),  $F$  increases with  $R_b$ , while it decreases with  $\alpha_c$ . When  $R_b = 0.95$  and  $\alpha_c = 0.05$ , or  $R_b = 0.90$  and  $\alpha_c = 0.10$  (the optimal resonant condition),  $F$  can attain values 57.67 and 29.31, respectively.  $F$  will rapidly decrease to less than 20 if  $R_b$  decreases and  $\alpha_c$  increases further. When  $R_b$  and  $\alpha_c$  satisfy the optimal resonant condition, the relation between  $\Delta\omega$  and  $\rho$  follows the curve in Fig. 3(b). When  $\Delta\omega$  is less than 1 MHz,  $F$  will reach values greater than 27; however, if  $\Delta\omega$  increases further to 10 MHz,  $F$  will decrease to 19.55. Therefore, when  $\Delta\omega$  is less than 1 MHz, the coupling loss  $\alpha_c$  should be decreased and the reflectivity  $R_b$  should be increased simultaneously to improve the resonant finesse  $F$ .

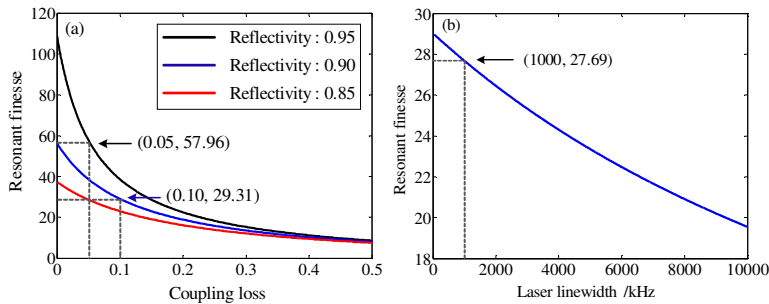


Fig. 3. Resonant finesse varies with different optical parameters: (a) reflectivity and coupling loss and (b) laser linewidth.

In Fig. 4, the effects of  $R_b$ ,  $\alpha_c$ , and  $\Delta\omega$  on the sensitivity  $\Delta\Omega$  are simulated and illustrated. Figure 4(a) plots the relationship between  $\Delta\Omega$  and  $R_b$ . In the region where the coupling loss  $\alpha_c$  is less than 0.1, when  $\alpha_c$  is constant,  $\Delta\Omega$  increases with  $R_b$ , and maximal sensitivity occurs in

this region. The maximal sensitivity of every curve is provided in the inset of Fig. 4(a), and different values of  $R_b$  correspond to different maximal sensitivities. When  $\alpha_c$  is in the range from 0.1 to 0.2, a slight difference can be observed between the two curves whose reflectivities are 0.90 and 0.85. The change of the sensitivity is larger for  $R_b = 0.95$ . When  $\alpha_c$  is larger than 0.2, the sensitivity increases monotonically with  $R_b$ . Here, a smaller  $R_b$  implies that more energy is available for importing into the resonator. This increase in energy can compensate for the influence of the larger coupling loss on the sensitivity. Therefore, if  $\alpha_c$  is larger, we can decrease  $R_b$  accordingly to effectively improve the sensitivity. The sensitivity is observed to decrease almost linearly as  $\Delta\omega$  increases when the optimal resonant condition is satisfied (Fig. 4(b)). It should be noted that  $\Delta\omega$  can significantly affect the sensitivity when its value is greater than 1 MHz. The sensitivity varies from  $0.031^\circ/\text{h}$  to  $0.07^\circ/\text{h}$  in the range of  $\Delta\omega$  plotted in Fig. 4(b). Therefore, if we want to obtain a higher sensitivity, a narrower linewidth laser source must be selected. Also to get a better performance of R-FOG, the coupling loss should be further reduced and the reflectivity should be determined properly simultaneously. According to the above analysis, the set of parameters we recommend is  $R_b = 0.9$ ,  $\alpha_c = 0.1$  and  $\Delta\omega = 30\text{kHz}$  with the theoretical sensitivity  $0.0314^\circ/\text{h}$ .

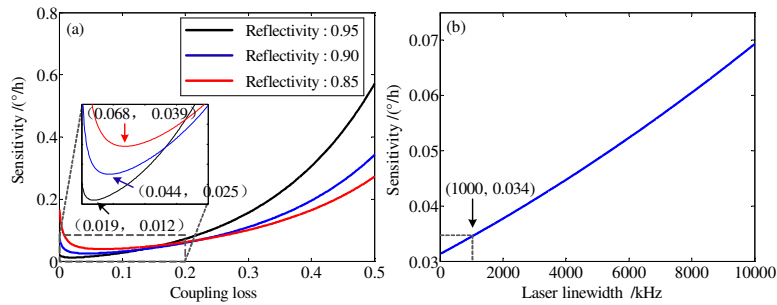


Fig. 4. Sensitivity varies with different optical parameters: (a) reflectivity and coupling loss and (b) laser linewidth.

### 3 Experimental research

A photograph of the HC-PBF FRR sample we fabricated is presented in Fig. 5(a). A scanning electron microscope (SEM) photomicrograph of the HC-PBF cross-section is shown in Fig. 5(b). The complete FRR is composed of a HC-PBF from NKT Photonics (HC-1550-PM-01), a panda PMF and the coupler based on the micro-optical structure. The coupler consists of a coupling lens and splitter. The size of the splitter is  $1.4\text{ mm} \times 1.4\text{ mm}$ . The length of the HC-PBF is 1.6 m. All of the elements are integrated together in a package to reduce external disturbances.

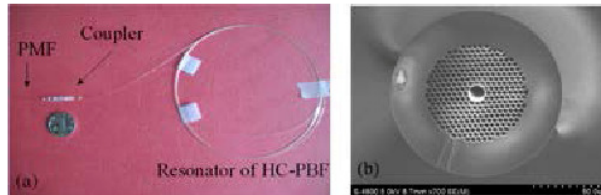


Fig. 5. (a) HC-PBF ring resonator based on micro-optical structure. (b) SEM photograph of a HC-PBF (cross-section).

The FRR was experimentally tested and the setup is illustrated in Fig. 6(a). One end of the FRR connecting with the laser serves as the input port, and a polarization-maintaining controller (PMC) is located between the input port and the laser source to adjust the polarization of input light. Another end of the FRR connecting with the PIN/FET detector is used to collect the output signal. By tuning the central frequency of the laser with a signal

generator, the output resonant curve was obtained using an oscillograph. The laser source had a central wavelength 1550.0 nm and its linewidth was less than 30 kHz, therefore, the influence of the laser linewidth on the performance of resonator can be neglected.

The experimental results are presented in Fig. 6(b). An obvious resonance is observed. The resonant finesse is 11.75 and the resonant depth is 0.087. According to Eq. (6), we can estimate that the sensitivity can reach  $0.6^\circ/\text{h}$ , which meets the tactical requirement. In addition, by substituting these two values into Eqs. (4) and (5), we obtain  $R_b = 0.9879$  and  $\alpha_c = 0.4107$ . The measured values of  $R_b$  and  $\alpha_c$  are found to be larger than the designed values. Two main reasons for this finding are (1) the geometrical parameters of the collimating lens are not optimal and (2) the locations of the coupler elements misaligned with each other.

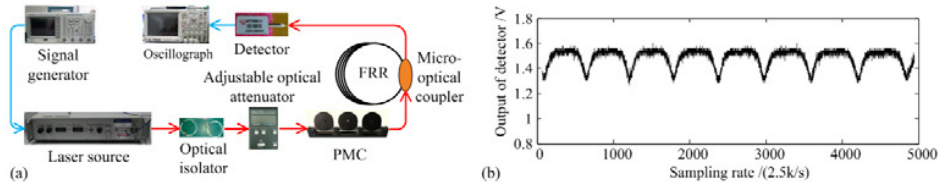


Fig. 6. (a) Experimental setup and (b) resonant curve of the HC-PBF ring resonator based on micro-optical structure.

The loss of the HC-PBF is relatively small. However, the obtained coupling loss is much larger than its theoretical counterpart. Therefore, the loss of the entire resonator is concentrated mainly in the coupler. Thus the reduction of coupling loss is critical for a better performance and, however, it is limited by the process capability. Thus it is necessary to modify the reflectivity of the highly reflective membrane. To obtain the highest sensitivity, the relation between  $R_b$  and the sensitivity was simulated for the case where the coupling loss is 0.4 (see Fig. 7). To obtain a high sensitivity,  $R_b$  must be reduced to 0.77. In this case, the theoretical sensitivity is  $0.153^\circ/\text{h}$  and improved by 22%.

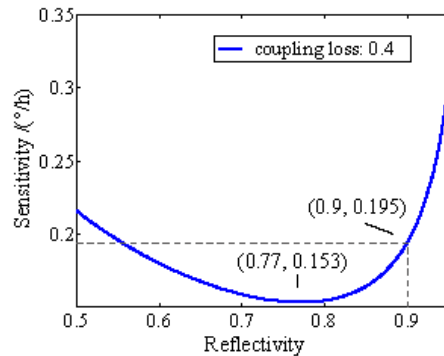


Fig. 7. Relation between  $R_b$  and the sensitivity.

#### 4 Conclusions

In the work, a novel HC-PBF ring resonator based on micro-optical structure is proposed. Its theoretical model is established and its transfer function is similar to a conventional FRR designed using a normal fiber. The highest sensitivity in theory,  $0.0314^\circ/\text{h}$ , can be realized when the reflectivity is 0.9, the coupling loss is 0.1 and the laser linewidth is 30 KHz. The fabricated sample is experimentally tested and the results indicate that the coupling loss is relatively larger and critical to the performance of FRR. An optimal sensitivity  $0.153^\circ/\text{h}$  can be reached by optimizing the designed parameters.

## **Acknowledgments**

This work was supported by the National Natural Science Foundation of China under Grant No. 61171004.